Control of Calcium Carbonate Crystallization by a Serum Protein

Problem Presenter: D. Bassett and J. Barralet (Strathcona Anatomy & Dentistry, McGill University)

Contributors: C.S. Bohun (UOIT), C.J.W. Breward (University of Oxford), H. Huang (York University), M. Morfin (University of Toronto), N. Nigam (McGill University), J. Phillips (McGill University), B. Tilley (Franklin W. Olin College of Engineering), M.J. Tindall (University of Reading), J.A.D. Wattis (University of Nottingham)

Report prepared by[1]**:** Mario Morfin, C. Sean Bohun, and Jonathan Wattis

Abstract. Calcium carbonate crystals occur in a variety of shapes, each morphology having differing physicochemical properties. This problem involves the formation of calcium carbonate crystals in a gas diffusion process. Experiments showed the formation of clear shapes in the presence of a serum protein. These structures appear to be formed from calcium carbonate fibers arranged in cones, fiber bundles, discs, and other shapes. Some characteristics of the crystals, such as the layering of self similar structures, suggest a process which regulates crystallization. Here we propose a mechanism for the formation of calcium carbonate fibers and their assembly in the complex structures. We describe this process in two systems of partial differential equations. We aim to simulate the growth of these crystals in order to understand the effect of the concentrations and diffusion of the different elements and compounds that are present in the reaction, in the global regulator of the crystallization process.

McGill 2.0kV 6.0mm x500 SE(U)   100um

[1] mario@math.utoronto.ca, sean.bohun@uoit.ca, Jonathan.Wattis@nottingham.ac.uk

1 Introduction

Calcium carbonate, $CaCO_3$, is one of the three most common biominerals, the other two being calcium phosphate and silica. When crystallised, $CaCO_3$ forms diverse morphologies with different mechanical, electrical and optical characteristics. This variety of morphologies makes calcium carbonate useful in industry. When biomineralization occurs, various proteins are found in mineralized tissues such as bone, teeth and shells. The presence of these proteins in the biomineralization process is known to effect the characteristics of the final crystal.

The problem posed is to describe the crystallization of calcium carbonate in a gas diffusion process. This process, which will be described in detail below, mimics the biomineralization of $CaCO_3$. It relies on the decomposition of ammonium carbonate to produce carbon dioxide and ammonia gas in a closed environment. The crystallization is achieved via the diffusion of carbon dioxide gas into a solution filled with calcium chloride.

It is well known that, in the absence of other agents, calcium carbonate will crystallize into its most stable form: rhombohedral microcrystals of calcite, see Figure 1 (left). In the experiments presented to the group, an external compound, a serum protein which we denote by P, was introduced to the solution of calcium carbonate. It is known that the serum protein, which is highly phosphorylated, is similar to those found in bone, serum and milk, and inhibits the formation of large calcium carbonate crystals. The aim of the experiment is to explore the effect of the serum protein on the crystallization process.

In the presence of serum protein under the conditions of our experiments, aggregate structures, such as fibres, cones, plate-like floating shapes and fibre bundles, were observed. These structures were formed as calcium carbonate fibre crystals bound together.

The crystals were found in the following configuration: the aggregate structures were formed in the aqueous solution, attached to the surface of the liquid. The cone tips and the binding point of the bundle were also attached to the surface, while the rest of the structure was suspended in the solution. Calcite was formed attached to the bottom of the vessel. Nanofibres were found loose at the bottom of the vessel after drying.
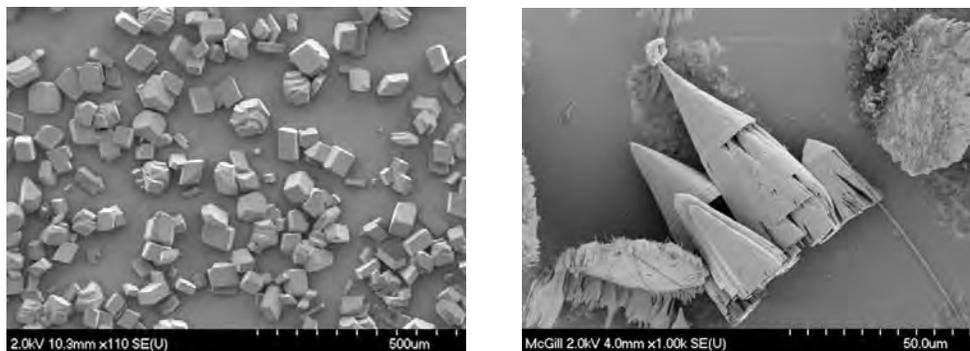
Figure 1 The image to the left shows rhombohedral calcite crystals. The presence of serum protein changes the morphology as illustrated by the image to the right which shows a beautiful set of crystallized cones.

Some global characteristics were observed. For example, in any one experiment, the cone-like shapes appear to be similar, in that they had a similar angle at each apex, even when embedded within each other. The lower boundary of the crystals, i.e. where the crystal stops growing, appear to be constant along separate aggregate structures. (See

Figure 1, right picture and Figure 4, right picture.) This suggests the existence of a global regulatory process.

In the present report, we propose a mechanism for the formation of calcium carbonate fibres and crystals in the complex structures described above. Also, we present two systems of partial differential equations (PDEs) which we use to simulate the growth of these aggregate structures. From the simulations, we attempt to understand the impact of the concentrations and diffusion of the various substances on this regulatory process.
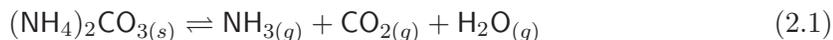
2 The experimental gas-diffusion process

2.1 Methodology. A simple gas diffusion method was used to precipitate calcium carbonate. It was carried out in a closed desiccator at room temperature. The serum protein was dissolved in 100 mM $CaCl_2$ aqueous solution and 1 ml of solution was placed in the reaction vessel. The reaction vessel was then covered with parafilm and punctured six times with a needle. Crushed ammonium carbonate was placed in a dish, covered with parafilm, then punctured in the same way, placed in the bottom of the desiccator. Typically the reaction was allowed to stand for three days, as this was deemed to be when the reaction had reached completion; however, some samples were kept for shorter (one day) and longer (twenty days) times. See Figure 2 for an illustration of the physical setup. Upon completion of the crystallization, the calcium carbonate was removed, dried and examined by X-ray diffraction, scanning and transmission electron microscopy (SEM and TEM).
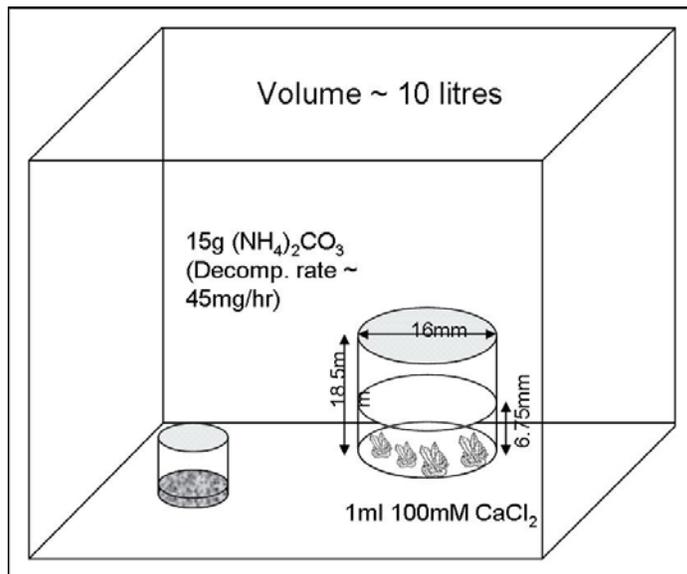
Figure 2 Experimental apparatus for the gas diffusion process.

2.2 Chemical reactions. The ammonium carbonate sublimation chemical reactions are

$$(NH_4)_2CO_{3(s)} \rightleftharpoons NH_{3(g)} + CO_{2(g)} + H_2O_{(g)} \qquad (2.1)$$

$$CO_{2(g)} + H_2O_{(l)} \rightarrow CO_3^{2-} + 2H^+ \qquad (2.2)$$

$$NH_{3(g)} + H_2O_{(l)} \rightarrow NH_4^+ + OH^- \qquad (2.3)$$

Carbon dioxide was released to the desiccator, and then dissolved in the solution forming dissolved carbon dioxide as well as carbonate ions (CO_3^{2-}) and H_3O^+. According to the diffusion equation, under these experimental conditions, it should take around five hours for these ions to diffuse to the bottom of the vessel. Carbonate ions then react, in the presence of protein, with the Ca^{2+} ions to form $CaCO_3$ in the aqueous solution, according to the reactions

$$CaCl_2 \rightarrow Ca^{2+} + 2Cl^- \tag{2.4}$$

$$Ca^{2+} + CO_3^{2-} \rightleftharpoons CaCO_3. \tag{2.5}$$

The protein is about 200nm long, it has a molecular weight of about 60 kDa, and it is highly phosphorylated. It is amphiphilic since its ends are hydrophobic whilst its centre is slightly hydrophilic. If present at high enough concentration in water, it forms micelles. In the presence of $CaCO_3$, in order to minimise energy, its ends will be in contact with $CaCO_3$ rather than water, thus we might expect the polymer to interact with crystal surfaces once the crystals grow to a large enough size.

2.3 Summary of experimental results. Two types of structures were observed after the crystallization process: nanofibres and aggregated structures (the former appear to be the building blocks of the latter). Nanofibres were between 1 and 2 μm wide, while the size of the aggregated structures were hundreds of times larger (up to 0.5 mm).

At low concentrations of the serum protein (between 0.1 mg/ml and 0.5 mg/ml), only nanofibres were observed. Cones and bundles of fibres were only found at protein concentrations above 1 mg/ml, see Figure 3 (right) and Figure 4 (left and right). At concentrations lower than 0.1 mg/ml, the fibrous structure was lost — see the left panel of Figure 3.
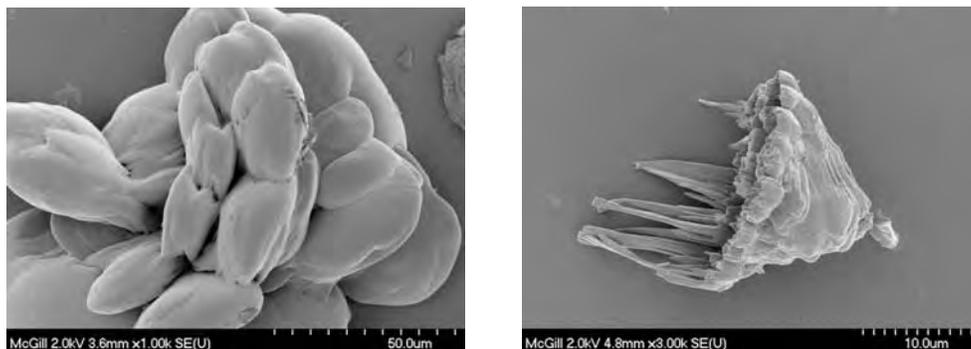
Figure 3 These pictures show the effect of low concentration of protein. On the left, the concentration is lower than 0.1 mg/ml (fibrous structure is lost); on the right, the concentration is 1 mg/ml.

The formation of the nanofibres and the aggregated structures is not simultaneous. It was observed that there are three phases of calcium ion uptake: 6 hours, 36 hours and 72 hours from the start of the reaction. The first detectable structures appear after around fifteen hours. Bundles and cones appear later, in the last phase of the experiment. Also, some calcite was crystallized at the bottom at the earliest stage of the experiment. These crystals were found attached to the vessel. Some nanofibres precipitated to the bottom, unattached to the vessel. (See Figure 4, left picture.) This suggest that the nanoparticles
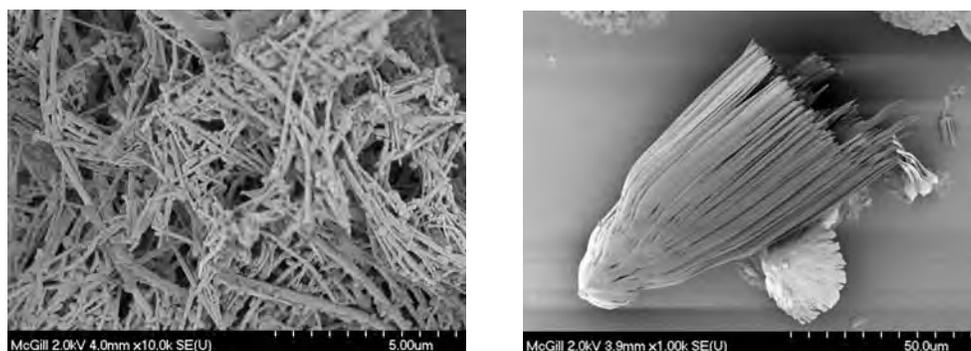
Figure 4 Individual fibres and an example of the bundling of fibres. The concentration of protein is 1 mg/ml.

were formed and assembled in the intermediate phase of the experiment. The remaining fibres fell down after drying.

We visualise cones as hanging vertically downwards from an upper point. The viscosity of the aqueous solution had a role to play as well. If we take a vertical transversal cut of one of the conical shapes, the line that defines the exterior of the crystal will not be straight in general; its concavity depends on the viscosity. Namely, as the viscosity increases, the cones appear to be more 'spread out' and have a larger angle at the tip. The shape of the bundles follows a similar pattern. However, the changes in viscosity did not alter the general shape of the aggregated structures, nor their global behaviours. See Figure 5.
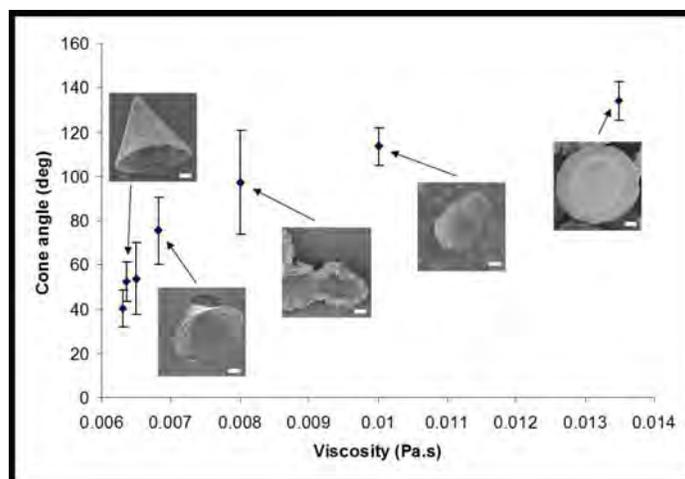
Figure 5 Changes in the opening angle of the fibre cones as a function of the viscosity of the aqueous solution.

The position of the water surface turned out to be important as well. A variation of the standard experiment was done in a very thin pipette, which was small enough that, if turned upside down, the water surface is preserved by surface tension, and the solution does not drop down. Two pipettes with the solution of protein and $CaCl_2$ were placed in the desiccator, one upside down and the other upright. The first did not show growth of crystals, while the other did. Other variations, such as rocking the containers, resulted in

the absence of crystals as well. This could simply be due to the fragility of the crystal structures.

This biomineralization-like process starts out with the diffusion of carbon dioxide into the protein solution. Since no other material is getting in or out the vessel, the time scales of the uptakes of the structures described above imply that they depend only on the concentration of each component. Therefore understanding these concentrations is one of the keys to understanding the interactions with respect to the crystallization process. This aggregation process is independent of the way the nanoparticles and the fibres are bound together.

Based on these observations, many interesting phenomena can be subjected to modeling. For instance, as observed before, The mechanism responsible for the crystallization must be responsible for the banding structure and the way clusters are formed, as well as the assembly of the self-similar structures in layers.

Our objective is to model the formation of calcium carbonate, with and without the protein. Then, considering the appropriate terms in the system, we simulate the uptakes of nanoparticles, the fibres and finally the crystal growth.

3 Mathematical modelling

3.1 Proposed mechanism. In this section, we propose a mechanism for the formation of the crystals. The two systems of PDEs that we present below describe this process. The key stages in the process are as follows:

1. Carbon dioxide dissolves into solution of water with calcium chloride and serum protein.
2. Carbonate ions combine with calcium ions to form calcium carbonate (which is insoluble).
3. Calcium carbonate, in the absence of a serum protein, forms large crystals, that is, the growth of crystals is not limited.
4. Calcium carbonate, in the presence of the serum protein, form nanoparticles. Though we do not model their shape or configuration, it is assumed that their morphology makes the nanoparticles bind into rather large filaments [9, 10]. This indicates some sort of growth-limiting effect of the serum protein.
5. When the concentration of nanoparticles reaches a critical level, they aggregate, or self-assemble, to form fibres. In the experiments, the serum protein was never fully consumed.
6. The fibres assemble to form sheets, bundles and cones. It is not clear whether this occurs after fibre-formation or whether the two processes occur simultaneously.

Our system of equations describes the three time stages of the problem, namely the diffusion of calcium and carbonate ions into the solution, the nucleation and growth of $CaCO_3$ crystals which may occur with interaction with the serum protein and, finally, the arrangement of the nanoparticles into crystallized superstructures.

3.2 Calcium carbonate formation and nanoparticles. We construct a system of PDEs that are one-dimensional in space, with the z-coordinate measuring depth from the top of the vessel; thus $z = 0$ corresponds to the top of the vessel. Here u and v are respectively the concentrations of calcium ions and carbonate ions at depth z and time t.

The initial conditions are as follows: first, there is no flow of any element or compound through the bottom of the vessel $z = L$. In addition, at the top of the vessel, we assume

Table 1 Summary of parameter values.

Parameter	Description	Value
L	Depth of container	6.75 mm
u_0	Initial concentration of calcium in vessel	50 ppm
v_{air}	Carbon dioxide concentration in air above vessel	387 ppm
h	Constant for dissolution of $CO_{2(g)}$	2×10^{-5} $\text{mol}\,\text{m}^{-2}s^{-1}$
α	Stoichiometic constant for crystal-protein ratio	3
P_0	Initial concentration of serum protein	$1\ \text{mg}\,\text{ml}^{-1}$
a	Inverse of diameter of nanoparticle X_p	1 nm
k_1	Reaction rate for $Ca + CO_3 \rightarrow CaCO_3$	1×10^{-5}
k_2	Reaction rate for $\alpha X + P \rightarrow X_p$	1×10^{-2}
k_3	Rate of fibre growth in model system 1	1
$\widehat{k_3}$	Rate of fibre growth in model system 2	2×10^{-5}
$\widehat{k_4}$	Rate of sidebranching in model system 2	2×10^{-4}
ε	Rate of new fibre nucleation in model system 2	2×10^{-3}
D_1	Diffusion constant for calcium ions, u	2 cm^2s^{-1}
D_2	Diffusion constant for carbonate ions, v	2 cm^2s^{-1}
D_4	Diffusion constant for microcrystals, X	1 cm^2s^{-1}
D_5	Diffusion constant for nanoparticles, X_p	1 cm^2s^{-1}

a Robin condition for the diffusion of $CO_{2(g)}$, with no carbon dioxide in the solution at time $t = 0$ and a positive atmospheric concentration, v_{air}. We will also assume uniform concentrations of calcium and protein initially in the solution. Hence we have

$$u(z,0) = u_0, \qquad u_z(0,t) = 0, \qquad v_z(0,t) = h(v_{\text{air}} - v(0,t)), \qquad (3.1)$$

$$v(z,0) = 0, \qquad u_z(L,t) = 0, \qquad v_z(L,t) = 0 \qquad (3.2)$$

with the constant of dissolution of $CO_{2(g)}$ given in Table 1.

We apply the law of mass action to the governing chemical equations (2.5), which can be written chemically as $u + v \xrightarrow{k_1} X$, to obtain the following system of coupled non-linear equations

$$\frac{\partial u}{\partial t} = D_1 \frac{\partial^2 u}{\partial z^2} - k_1 uv, \qquad\qquad \frac{\partial v}{\partial t} = D_2 \frac{\partial^2 v}{\partial z^2} - k_1 uv, \qquad (3.3)$$

where D_1 and D_2 are the diffusion coefficients for calcium and carbonate ions respectively, and k_1 is the reaction term for the calcium and carbonate ions to combine and form the insoluble crystal, X, whose concentration we denote by $X(z,t)$.

Denoting the protein concentration by $P(z,t)$, the boundary and initial conditions for X and P describe the fact that neither can escape from the top or bottom of the reaction vessel. Whilst there is no crystal present at $t = 0$, the protein is present, at some concentration, P_0 distributed uniformly, hence we have

$$X_z(0,t) = 0, \qquad X_z(L,t) = 0, \qquad X(z,0) = 0, \qquad (3.4)$$

$$P_z(0,t) = 0, \qquad P_z(L,t) = 0, \qquad P(z,0) = P_0. \qquad (3.5)$$

The second set of PDEs describe the formation of $CaCO_3$ when they interact with the serum protein, which is present at concentration $P(z,t)$. The chemical model we wish to describe

is $\alpha X + P \xrightarrow{k_2} X_p$, where X_p denotes a nanocrystal of calcium carbonate which is large enough to have adsorbed at least one protein molecule onto its surface. Hence,

$$\frac{\partial P}{\partial t} = D_3 \frac{\partial^2 P}{\partial z^2} - k_2 X^\alpha P, \qquad\qquad \frac{\partial X}{\partial t} = D_4 \frac{\partial^2 X}{\partial z^2} - k_2 X^\alpha P + k_1 uv, \qquad (3.6)$$

where D_3 and D_4 are the diffusion coefficients, k_2 is the combined reaction term for the nucleation and growth of a calcium carbonate crystal and its subsequent combining with protein. Rather than go to the complexity of modelling clusters of the full range of sizes, we go straight to an approximation in which many particles are assumed to interact to form a much larger complicated structure. This can be derived in a more rigorous fashion, as analysed in other work [3, 5], and has been used successfully in a number of applications from surfactant flow [1, 2] to other models of nucleation, competition and inhibition [4, 11].

The third part of the model has been approached in two different ways, these are presented in the next two subsections. The first model's growth occurs only at the tips, whilst the second takes into account the possibility that fibres may branch as they grow, giving rise to triangular surfaces.

3.3 Formation of fibre nanocrystals and fibres: system 1. We assume that fibres are initiated at the top surface and grow vertically downwards, so a fibre of length q ends at a depth $z = q$. Let X_p be the concentration of nanoparticles and $Y(z, t)$ the number of fibres of length z ending at depth z at time t. We assume that nanoparticles can move by diffusion, but that fibres are fixed. Nanoparticles are created by the process $\alpha X + P \xrightarrow{k_2} X_p$ discussed above, hence X_p is determined by an equation similar to (3.6):

$$\frac{\partial X_p}{\partial t} = D_5 \frac{\partial^2 X_p}{\partial z^2} + k_2 X^\alpha P - k_3 a X_p Y, \qquad (3.7)$$

where D_5 is the diffusion coefficient of the nanoparticles X_p, k_2 is as before, and k_3 is the reaction term for the nanoparticles and calcium carbonate fibres. The derivation of an equation for $Y(z, t)$ is more complex.

The quantity $Y(z, t)$ can only change if there are fibres that end at $z - \delta$ (for some small $\delta \ll 1$). Because fibres grow downwards, we must have $Y(z - \delta) > Y(z)$. In a discrete approximation to the system, we let $Y(n\Delta z, k\Delta t)$ be the number of fibres of length $n\Delta z$ at time $k\Delta t$. In the next time interval, a particle X_p will be added with probability which depends linearly on the concentration X_p, hence we denote this probability by pX_p. Incorporation of tips of length $n\Delta z$ is done at the expense of tips located at $(n-1)\Delta z$. Thus we have

$$Y(n\Delta z, (k+1)\Delta t) = Y(n\Delta z, k\Delta t) - pX_p Y(n\Delta z, k\Delta t) + pX_p Y((n-1)\Delta z, k\Delta t). \qquad (3.8)$$

Taking the limits $\Delta z \to 0$, $\Delta t \to 0$ with $\Delta z \sim \Delta t$, and defining $k_3 = p \lim_{\Delta t \to 0}(\Delta z / \Delta t)$, we obtain

$$\frac{\partial Y}{\partial t} = -k_3 X_p \frac{\partial Y}{\partial z}. \qquad (3.9)$$

Hence fibres grow at the rate $k_3 X_p$, with k_3 having units of $[k_3] =$ length per concentration per time. For (3.7) we require the units of $k_3 a X_p Y$ to match that of $\partial X_p / \partial t$. Therefore the units of the constant 'a' must be inverse length. In fact $1/a$ can be thought to correspond to the diameter of an X_p nanoparticle.

In this system, fibres grow only at the tip, that is, there is no side-branching. In this formulation, k_3 is the reaction term for the nanoparticles and the tips' aggregated structure.

3.4 Formation of fibre nanocrystals and fibres: system 2. In this formulation, as well as fibres growing from the surface downwards with growth only occurring at their lower ends, we permit the formation of new fibres anywhere in the vessel where there are sufficient nanoparticles (X_p), and we allow growing fibres to sidebranch, so that the aggregated structures become wider at the bottom than the top.

Let $X_p(z,t)$ be as before, but now $Y(z,t)$ is the *mass* of fibres at depth z; we assume that two nanoparticles colliding can initiate the growth of a new fibre – which will be a small effect, hence the rate constant is taken to be ε. More important is the extensional growth of existing fibres, which occurs with a rate constant $\widehat{k}_3$ ($[\widehat{k}_3]=$ length per concentration per time) and the side-branching which occurs at a rate $\widehat{k}_4$ ($[\widehat{k}_4]=$ per concentration per time). Side-branching causes the crystals to become wider further down the vessel. In accordance with (3.7) and (3.9) one has in this case

$$\frac{\partial X_p}{\partial t} = D_5 \frac{\partial^2 X_p}{\partial z^2} + k_2 X^\alpha P - \widehat{k}_3 a X_p Y - \varepsilon X_p^2 - \widehat{k}_4 X_p Y, \tag{3.10}$$

$$\frac{\partial Y}{\partial t} = -\widehat{k}_3 X_p \frac{\partial Y}{\partial z} + \varepsilon X_p^2 - \widehat{k}_4 X_p Y, \tag{3.11}$$

where the first term of the latter equation stands, as before, for the growth of the fibres. Typically we expect $\varepsilon < \widehat{k}_4 < \widehat{k}_3 a$. The boundary conditions for (3.10)–(3.11) are all zero flux and the initial conditions are also zero, namely

$$X_{p,z}(0,t) = 0, \qquad X_{p,z}(L,t) = 0, \qquad X_p(z,0) = 0, \tag{3.12}$$

$$Y_z(0,t) = 0, \qquad Y_z(L,t) = 0, \qquad Y(z,0) = 0. \tag{3.13}$$

3.5 Diffusion constants and other observations. Now we face the problem of estimating the constants for the various processes. These rates are known for the formation of calcium carbonate in alkaline environments, but not for environments where the serum protein is present; in these cases they have to be inferred. Rate constants are extracted from time dependent concentration profiles determined from experiment. Such profiles are depicted in Figure 6.

In the case of α, we set a value of 3, instead of 300, since for large α the equations become too stiff for the numerical method used. However, we can infer the results for large α. This will be detailed below. We also estimated the rest of the unknown coefficients, using similar principles.

4 Results

The systems of PDEs were solved using MatLab 7.5. The graphs below show the concentration of each component in the time-space phase plane. The color scale goes from blue to red, where blue signifies the absence of the component, and red the highest concentration.

4.1 Formation of fibre nanocrystals and fibres: system 1. Here we solve equations (3.1)–(3.9). First we present the solution of the system in the absence of protein, see Figure 7. The concentrations of calcium, carbonate ions, and calcium carbonate crystals conform to experimental observation. That is, nearly uniform production of calcium carbonate microcrystals with carbonate diffusing into solution from the position $z = 0$. We now compare Figures 7 and 8, the latter having protein in the solution. In both cases, the concentration of calcium decays through the experiment but is always nearly uniform through the vessel, the concentration of carbonate starts at zero and increases, initially
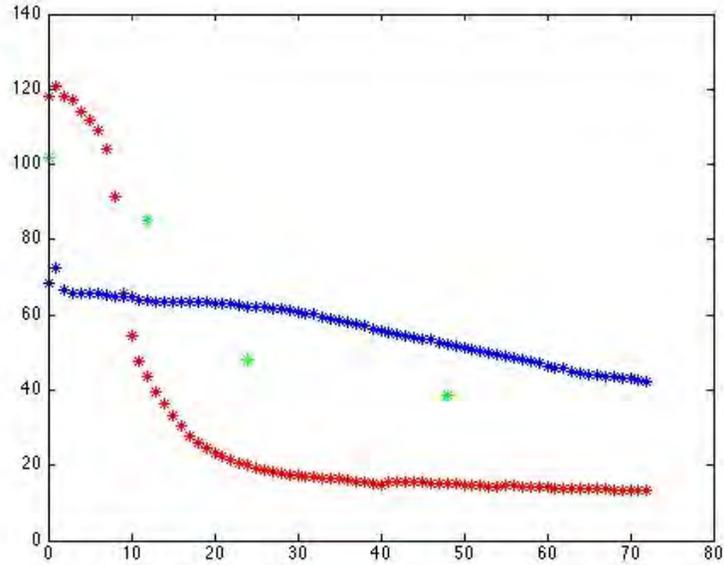
Figure 6 This graph shows the concentration of Ca^{2+} in the solution plotted against time for the cases with (red) and without (blue) protein. Without protein the concentration falls very slowly whereas with protein there is a significant decrease at about $t = 10$. The green data points are more careful measurements which compensate for the build up of $CaCO_3$ on the probes. These values are acquired less frequently (isolated data at $t = 10, 25, 50$).

from the top of the vessel, and always has a significant gradient from top to bottom of the vessel. The concentration of calcium carbonate has similar behaviour, although with a less pronounced gradient.

In Figure 8, we see the concentration of nanocrystals, fibres and the consumption of the protein in accordance with the first system of PDEs, where the initial concentration of the protein is not zero. In this simulation, the protein is consumed uniformly, but the nanocrystals at the top of the vessel are used first in the assembly of aggregated structures (fibres). In this case the assembly of nanocrystals into fibres occurs so rapidly that we see the formation of fibres from the top of the vessel, and never observe any significant concentration of nanocrystals, except for midway through the simulation when there is a small concentration at the bottom of the vessel. They cannot attach to fibres, because at this point in the simulation there are only fibres at the top of the vessel. Note that fibres grow monotonically.

Now we test the results of the simulation by varying the concentration of protein, and find results consistent with the experimental observations described above. At lower protein concentrations, it will take longer for the crystals (X) to interact with protein forming the nanoparticles X_p. Hence the formation of fibres would also be delayed; see Figure 9 top. An additional process in the experiment which has yet to be built into our models is that the crystals would grow larger before having their growth inhibited by the protein, and hence there would be fewer, but larger nanoparticles to form the fibres. On the other hand, if the
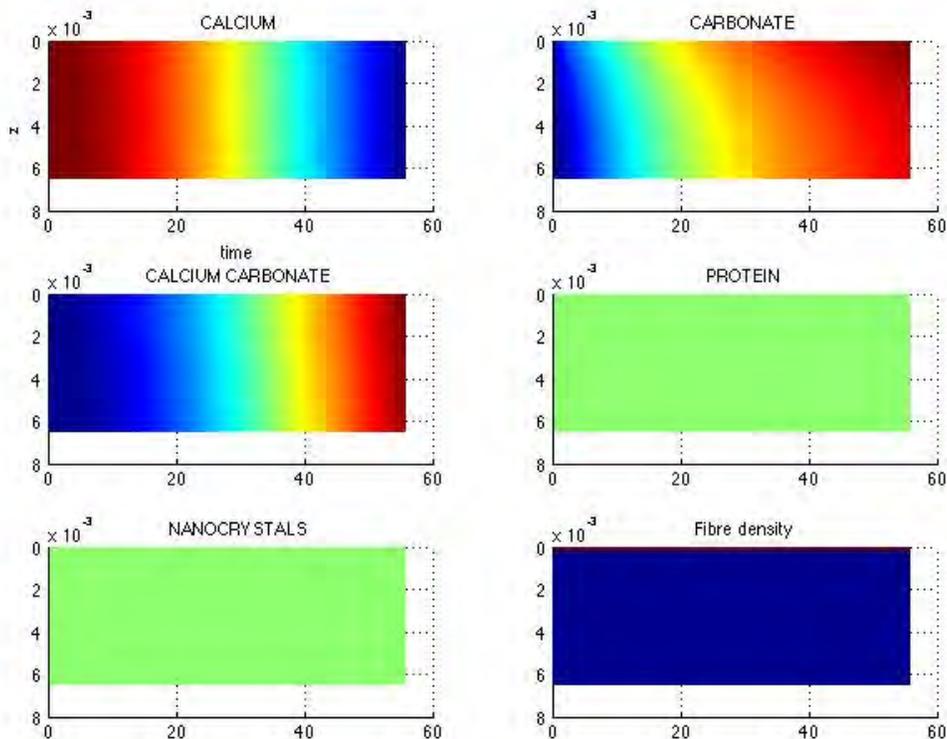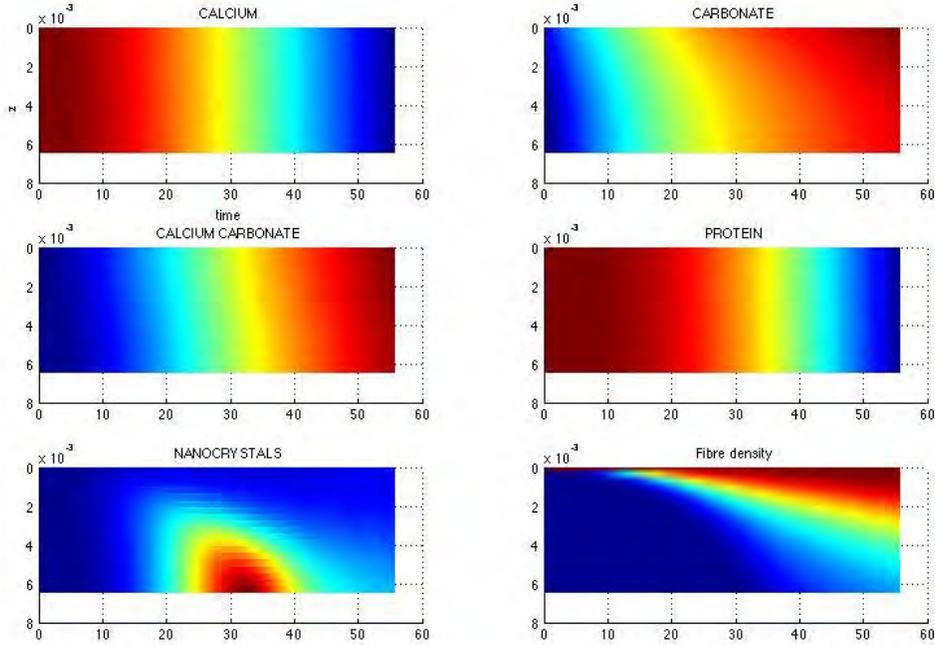
Figure 7 Solution of (3.1)–(3.9) without the addition of any protein. In this situation calcium chloride forms throughout the length $0 < z < L$.

concentration of protein is higher, the increase in fibre density occurs sooner, due to the more rapid formation of the X_p nanoparticles; see Figure 9 bottom.

As pointed out above, we have set α to 3, instead of 300, since for large α the equations become too stiff for the numerical method used. This parameter, determines the size of the nanoparticle. If its value increases, more calcium carbonate would be needed to form the aggregated structures. However, the global behaviour of the system would remain unaffected, and differences in timescales caused by changing α can be compensated for by simultaneously changing k_2.

4.2 Formation of fibre nanocrystals and fibres: system 2. Here we solve equations (3.1)–(3.6) and (3.10)-(3.13). Considering the possibility of branching allows us to describe other characteristics that we could not see using the first system. For a small amount of side branching the concentration profiles of the various species are not suprisingly quite similar to Figure 8 and are omitted for brevity. When nucleation of new fibres is significant in the model, we obtain a much clearer front in the formation of fibres as evidenced in Figure 10.

4.3 Effect of variations in viscosity. Recall that the viscosity of the aqueous solution did not alter the growth of the fibres, but did change the shape of the conical aggregate

Figure 8 Solution of (3.1)–(3.9) with the addition of a small amount of serum protein. Notice that the protein depletes uniformly in space. Nanocrystals form throughout but are incorporated into fibres starting at the top of the vessel.

(which we are not concerned with in this model). Since our model has no viscosity parameter, we model the change by changing the diffusion constants, and noting that these are given by $D = k_B T / 6\pi a \eta$, where k_B is Boltzmann's constant, T is temperature, a is the radius of the diffusing particle and η is the viscosity. Hence a doubling viscosity corresponds to reducing all the diffusion constants by a factor of two. Changing the viscosity had no appreciable effect for system 1 or system 2 with small side branching. However for system 2 with significant side branching, the crystallization front of both the nanoparticles and fibres is smoothed out by this change in viscosity; see Figure 11.

5 Discussion

We have formulated a model for the concentrations of the various species of ion, protein, microcrystals, and larger scale crystal complexes present in the system as a function of depth in the vessel, which describes their variation through the time course of the experiment. The models have the form of a coupled system of partial differential equations with parameters which we have derived from crude calculations based on experimental data. The ordering of events, and predicted form of the solution matches well with the observed data, although the model lacks the spatial resolution to describe the precise geometry of structures formed. We speculate that this structure may be related to the properties of the actual molecular level details of the protein present in solution.
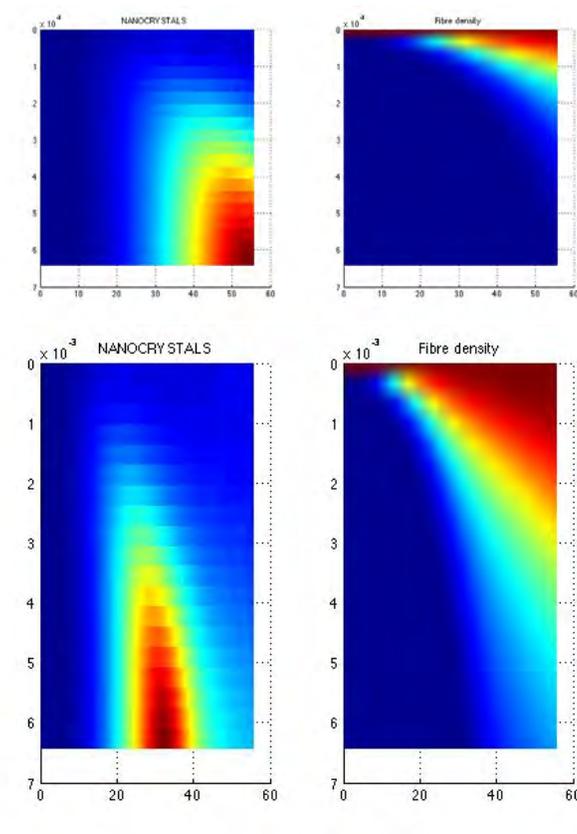
Figure 9 The effect of varying the initial protein concentration. Above the initial protein is 0.5 units, and below the initial protein is 2 units. Compare these with Figure 8, where the concentration is 1 unit.

We predict the presence of a diffusive wave of calcium carbonate which travels down through the reaction vessel. Serum protein interacts with these particles to form microcrystals coated in protein that then self-assemble into bundles of fibres which occasionally undergo side-branching. Side-branching forces the growing surface to become wider the further down the vessel it grows, causing an inverted cone-shaped structure to form.

Our model does not capture the geometry of the described aggregation phenomena beyond the fibres; namely, the ensemble of bundles and cones is not described. However, we can derive some conjectures that are consistent with the models described above, and the experimental data. For instance, at moderate concentrations of protein, fibres should grow in bundles, with a distribution of lengths. At intermediate concentrations, the fibres should grow to a length where secondary effects (competition of nucleation vs. increasing electrostatic energy) inhibit further growth. Under these conditions, cones will appear. Finally, for large concentrations of protein, nucleation should proceed on the inner surfaces of cones, and banding should appear. There are thus many questions which this report leaves open for further study.
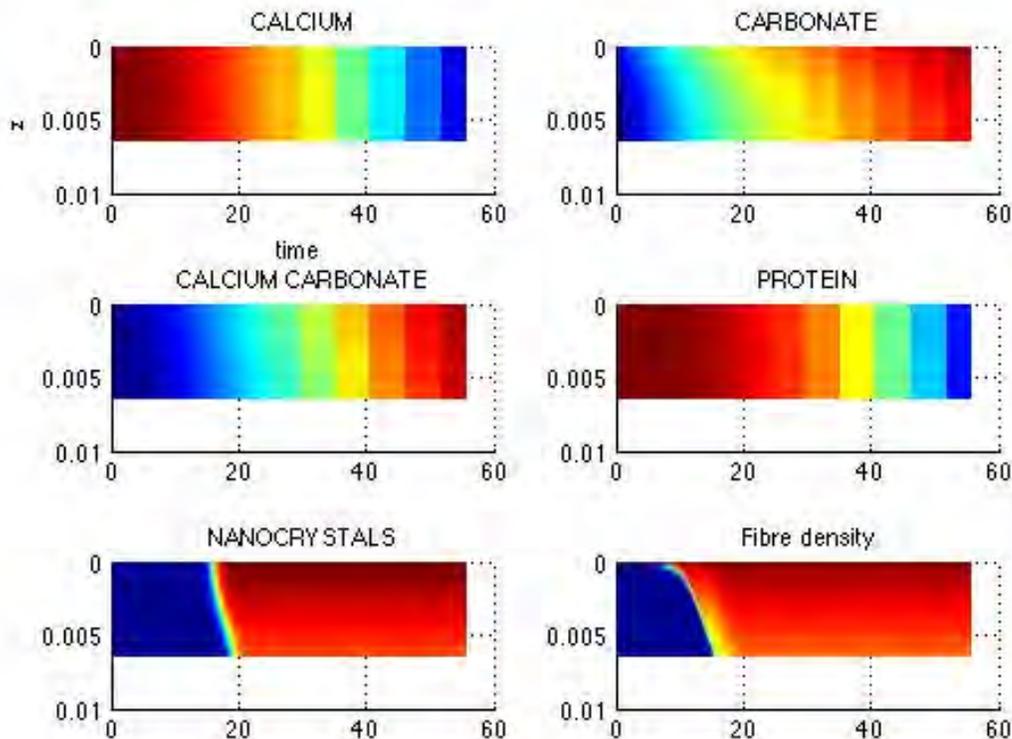
Figure 10 Solution to (3.1)–(3.6) and (3.10)-(3.13) when there is a significant amount of side branching. Compare to Figure 8 where no side branching occurs.

References

[1] C.G. Bell, C.J.W. Breward, P.D. Howell, J. Penfold and R.K. Thomas, *Macroscopic modeling of the surface tension of polymer–surfactant systems*, Langmuir **23** (2006), 6042–6052.

[2] C.J.W. Breward and P.D. Howell, *Straining flow of a micellar surfactant solution*, Euro. J. Appl. Math. **15** (2004), 511–531.

[3] C.D. Bolton and J.A.D. Wattis, *Generalised coarse-grained Becker-Doring equations*, J. Phys. A: Math. Gen. **36** (2003), 7859–7888.

[4] C.D. Bolton and J.A.D. Wattis, *The Becker-Doring equations with input, competition and inhibition*, J. Phys. A: Math. Gen. **37** (2004), 1971–1986.

[5] P.V. Coveney and J.A.D. Wattis, *Analysis of a generalized Becker-Döring model of self-reproducing micelles*, Proc. Roy. Soc. Lond. A **452** (1996), 2079–2102.

[6] S. Hayashi, K. Ohkawa, Y. Suwa, T. Sugawara, T. Asami and H. Yamamoto, *Fibrous and helical calcite crystals induced by synthetic polypeptides containing O-phospho-L-serine and O-phospho-L-threonine*, Macromolecular Bioscience **8** (2008), 46–59.

[7] X. Liu, B. Liu, Z. Wang, B. Zhang, and Z. Zhang, *Oriented vaterite $CaCO_3$ tablet-like arrays mineralized at air/water interface through cooperative regulation of polypeptide and double hydrophilic block copolymer*, J. Phys. Chem. C **112** (2008), 9632–9636.

[8] T. Somasundaram, M. in het Panhuis, and R.M. Lynden-Bell, *A simulation study of the kinetics of passage of CO_2 and N_2 through the liquid/vapor interface of water*, J. Chem. Phys. **111** (1999), 2190–2199.
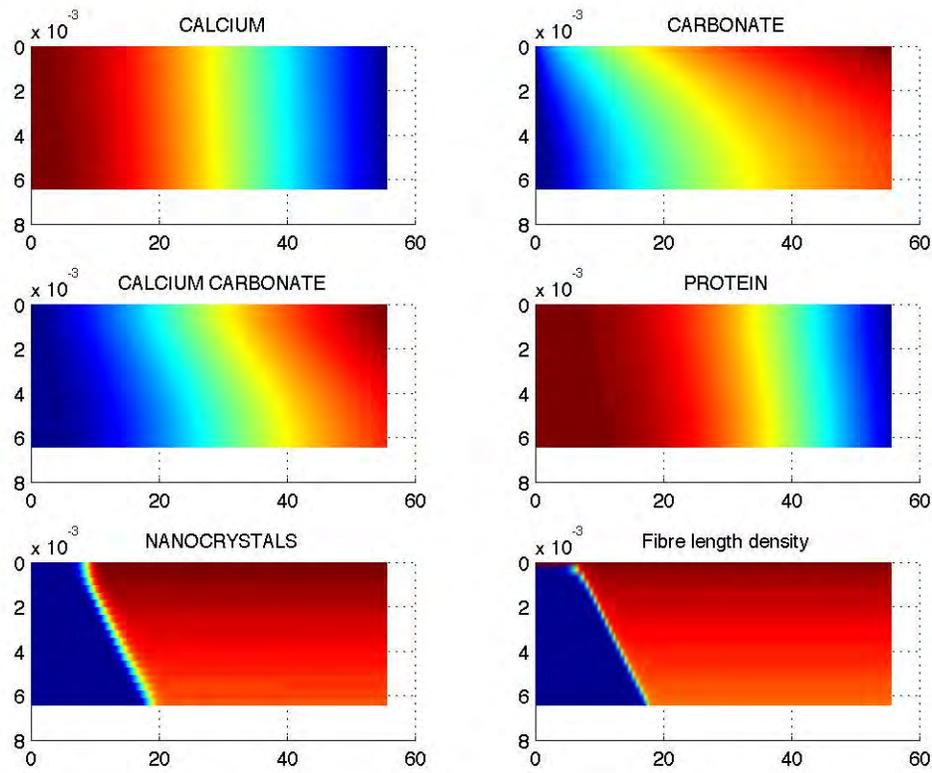
Figure 11 Solution to (3.1)–(3.6) and (3.10)-(3.13) with a solution of twice the viscosity which is simulated by halving all of the diffusion coefficients. The smoothing out of the crystallization fronts is evident when compared to Figure 10.

[9] T. Wangu, A. Reinecke, and H. Cölfen, *In situ investigation of complex* $BaSO_4$ *fiber generation in the presence of sodium polyacrylate. 2. crystallization mechanisms*, Langmuir **22** (2006), 8986–8994.

[10] T. Wangu and H. Cölfen, *In Situ investigation of complex* $BaSO_4$ *fiber generation in the presence of sodium polyacrylate. 1. kinetics and solution analysis*, Langmuir **22** (2006), 8975–8985.

[11] J.A.D. Wattis and P.V. Coveney, *Generalised nucleation theory with inhibition for chemically reacting systems*, J. Chem. Phys. **106** (1997), 9122–9140.